Jurnal Teknologi

Full Paper

NUMERICAL INVESTIGATION OF BIOFOULING ROUGHNESS IMPACT ON THE PERFORMANCE OF PROPELLER

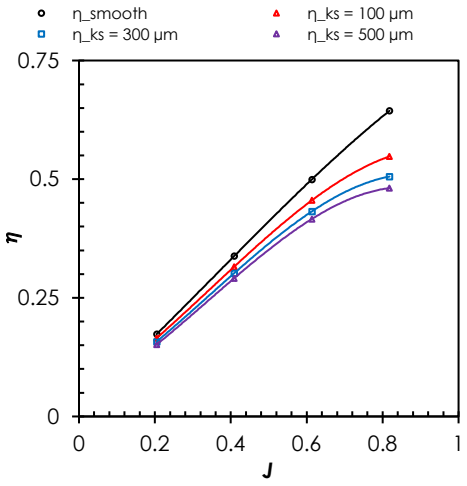
Berlian Arswendo Adietya[a], Muhammad Luqman Hakim[a]*, Tajussalatin Arvin Mertosono[a], Andi Trimulyono[a], Samuel[a], Tuswan[a], Ahmad Firdhaus[a], Ocid Mursid[a,b]

[a]Department of Naval Architecture, Faculty of Engineering, Universitas Diponegoro, Semarang, Indonesia 50275
[b]Department of Naval Architecture, Ocean and Marine Engineering, University of Strathclyde, Glasgow, UK G4 0LZ

Article history
Received
15th August 2025
Received in revised form
27th December 2025
Accepted
27th December 2025
Published
1st November 2026

*Corresponding author
mluqmanhak@lecturer.undip.ac.id

Graphical abstract



Abstract

Biofouling-induced surface roughness is a critical issue affecting the hydrodynamic performance of marine propellers, leading to increased energy consumption and emissions. This study investigates the effects of varying roughness heights on the thrust, torque, and open water efficiency of a B-series B4-70 marine propeller using Computational Fluid Dynamics (CFD). A wall-function-based roughness model was implemented within the RANS-SST turbulence framework to simulate realistic fouling scenarios while maintaining computational efficiency. The results demonstrate that surface roughness significantly decreases thrust and efficiency while increasing torque. At a roughness height of 500 μm, thrust losses reached up to 18% and efficiency dropped by nearly 2.5% at high advance coefficients, while torque increased by over 10%. These performance degradations are attributed to elevated wall shear stress and altered pressure distribution across the blade surfaces. The findings highlight the importance of maintaining clean propeller surfaces to reduce hydrodynamic losses, fuel consumption, and operational emissions in maritime applications.

Keywords: Biofouling, Surface Roughness, Propeller Performance, CFD Simulation, Hydrodynamic Efficiency.

© 2026 Penerbit UTM Press. All rights reserved

1.0 INTRODUCTION

Various measures are being explored to reduce emissions in the marine engineering sector, as addressing them is crucial for global climate action. Some of these efforts include designing ships with low-resistance hull forms [1–4], optimizing sailing routes to reduce travel time [5,6], improve propulsor [7–9] and fuel usage [10,11], adopting low-emission engines [12], and integrating renewable energy technologies onboard [13–16]. Among these strategies, one particularly practical and effective approach is maintaining clean hull and propeller surfaces to prevent biofouling. Hull roughness caused by biofouling significantly increases hydrodynamic drag, forcing the engine to consume more power to maintain the same speed. Studies have shown that severe biofouling can raise fuel consumption by more than 40% in extreme cases, thereby exacerbating CO_2 emissions from ships [17–19].

Biofouling significantly degrades a ship's hydrodynamic performance by increasing hull drag.

DOI: https://doi.org/10.11113/jurnalteknologi.v89.25357

The accumulation of organisms like algae and barnacles on wetted surfaces causes surface roughness, disrupting water flow and raising frictional resistance [20]. This condition leads to increased fuel use and operational costs if left untreated [21]. Experimental and numerical studies confirm this effect. Schultz et al. [22] found that macrofouling can raise total resistance by up to 60%, while CFD simulations by show roughness-induced drag increases of 10–30%, depending on fouling severity and distribution [23–26]. These drag increases demand more propulsion power, leading to higher emissions and reduced vessel efficiency.

Biofouling does not only affect the hull but also impairs critical propulsion components like the propeller. When marine organisms such as barnacles and algae attach to the propeller surface, they alter its smoothness and geometry, reducing hydrodynamic efficiency [27]. Unlike flat hull surfaces, propeller blades are carefully designed to convert rotational energy into thrust [28], and fouling disrupts this flow, causing unbalanced patterns, higher resistance, and potentially damaging vibrations [29]. CFD studies have shown that biofouling reduces thrust and increases torque coefficients, thereby lowering open-water efficiency [30,31]. The impact worsens with longer exposure and thicker fouling [32,33]. Changes in surface pressure, wall shear stress, and vortex structures lead to greater power demand and fuel use [34]. Due to its complexity, propeller fouling is harder to monitor and clean than hull fouling, often requiring costly dry-docking. Regular inspection and maintenance are crucial to minimize hidden efficiency losses [35].

Based on foil theory, a propeller functions similarly to a rotating hydrofoil, generating lift (thrust) and drag (torque) [36]. Efficiency is defined by the ratio of useful thrust to required torque [37]. Under clean conditions, blade geometry and smoothness maximize lift and minimize drag [38]. However, biofouling introduces roughness that increases drag, raising torque demand and reducing efficiency, while also affecting lift characteristics [39,40]. The fouling disrupts boundary layers, alters pressure distribution, and shifts angles of attack, causing premature flow separation, reduced lift, or vortex shedding [41]. Changes in lift can be as impactful as drag increases, further reducing efficiency [42]. Thus, biofouling's hydrodynamic penalties involve complex lift and drag interactions, making it essential to consider both when evaluating propeller performance.

Therefore, this study aims to numerically investigate the effects of biofouling-induced surface roughness on propeller performance, specifically focusing on the commercially prevalent Wageningen B-series B4-70 propeller characterized by wider blade (foil) area [43]. A Computational Fluid Dynamics (CFD) approach incorporating a modified wall-function roughness model is employed to realistically model the hydrodynamic effects of surface roughness. Unlike traditional methods that require fully resolved roughness geometries, this approach efficiently captures the influence of roughness on wall shear stress, boundary-layer behavior, and pressure distribution with lower computational cost. By systematically varying the roughness height, the study evaluates its impact on thrust, torque, and open-water efficiency, providing insight into the hydrodynamic performance degradation of biofouled propeller blades used in commercial vessels.

2.0 METHODOLOGY

2.1 Research Object and Variables

This research focuses on investigating the hydrodynamic implications of biofouling on a widely used commercial marine propeller, specifically the Wageningen B-Series type B4-70 [44,45]. This propeller was selected due to its extensive application in maritime operations, robust design, and its sensitivity to hydrodynamic performance alterations caused by biofouling. The geometry and operational characteristics of the propeller used in this study are summarized in Table 1, outlining parameters such as dimensions, rotational properties, and blade configuration.

Table 1 Parameters of the Wageningen B-Series B4-70 Propeller Model employed in this research

Parameter	Value
Diameter [m]	0.3
Pitch Ratio (P/D)	1.2
Area Ratio (A_e/A_o)	0.70
Revolution [rpm]	489
Rotation	Left-handed (CCW)
Number of Blade (Z)	4

To simulate realistic biofouling conditions, the research incorporates various roughness intensities, reflecting different stages and severities of marine fouling typically observed in operational environments, as presented in Table 2. These variations facilitate the investigation into how surface roughness impacts critical flow characteristics around the blades, including boundary layer disturbances, wall shear stress changes, and flow separation events. The operational scope is defined through carefully chosen values of the advance coefficient, representing typical operational scenarios encountered in maritime practices.

Table 2 Variation Parameters used in this study

Parameter	Values
Roughness Variation (k_s) [µm]	100; 300; 500
Advance Coefficient (J)	0.2; 0.4; 0.6; 0.8

DOI: https://doi.org/10.11113/jurnalteknologi.v89.25357

The selected roughness heights (k_s = 100–500 μm) are intended to represent practical biofouling conditions commonly observed on marine propellers, ranging from light surface fouling to more severe roughness levels. This range is consistent with values reported in previous experimental and numerical studies on propeller and hull biofouling. The advance coefficient range (J = 0.2–0.8) was chosen to cover typical operating conditions of the Wageningen B-series B4-70 propeller, encompassing heavily loaded conditions at low J and light-load or cruising conditions at higher J values.

Figure 1 and Figure 2 visually illustrate the geometry and key design features of the propeller model, highlighting aspects particularly relevant to its hydrodynamic performance when subjected to biofouling-induced roughness.

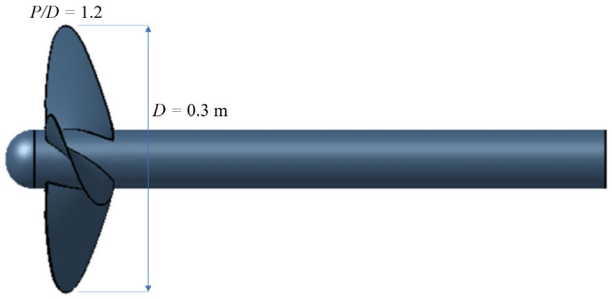


Figure 1 Side view of the Wageningen B-series B4-70 propeller model showing the propeller diameter (***D***) and pitch ratio (***P/D***) used in this study.

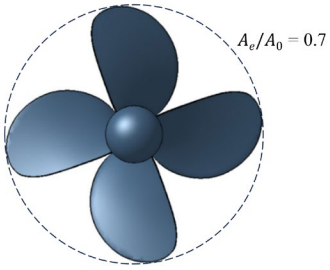


Figure 2 Rear view of the Wageningen B-series B4-70 propeller model illustrating the blade geometry, expanded blade area (Ae), area ratio (Ae/Ao), and number of blades (Z).

2.2 Propeller Theory

The performance of marine propellers is commonly evaluated using non-dimensional coefficients that describe thrust, torque, and efficiency as functions of operating conditions. These coefficients allow for the systematic comparison of different propeller designs and operating scenarios, independent of scale. In hydrodynamic analyses and numerical simulations, they serve as key performance indicators for assessing how effectively a propeller converts rotational energy into forward thrust.

The thrust coefficient (K_T) and torque coefficient (K_Q) are defined respectively in Equations (1) and (2). Where, T is thrust, Q is torque, n is rotational speed (rev/s), D is propeller diameter, and ρ is the fluid density. These coefficients describe the normalized force and moment produced by the propeller and are essential in determining how propeller performance scales with size and speed [46].

$$K_T = \frac{T}{\rho n^2 D^4} \tag{1}$$

$$K_Q = \frac{Q}{\rho n^2 D^5} \tag{2}$$

The advance coefficient (J) is another fundamental parameter, defined in Equation (3). Where, V_A is the advance velocity, representing the inflow speed relative to the propeller. This coefficient encapsulates the operating condition of the propeller, relating inflow velocity to rotation rate and diameter. Varying J allows one to observe how the propeller behaves under different loading conditions—from low advance (high thrust, e.g., acceleration) to high advance (cruising conditions).

$$J = \frac{V_A}{nD} \tag{3}$$

The open water efficiency (η) is expressed in Equation (4). Efficiency quantifies how effectively the input torque is converted into useful thrust. High efficiency indicates minimal energy losses due to viscous effects and flow separation, and is a critical metric in optimizing fuel consumption and overall vessel performance [47].

$$\eta = \frac{J}{2\pi} \cdot \frac{K_T}{K_Q} \tag{4}$$

In the context of this research, these coefficients are used to validate the numerical model against the well-documented Wageningen B-series experimental results. The agreement in K_T, K_Q, and η, across a range of J values, confirms the accuracy of the CFD simulation in predicting propeller behavior. Moreover, these coefficients are instrumental in assessing the impact of surface roughness due to biofouling on hydrodynamic performance.

2.3 Numerical Modeling

2.3.1 Mathematical Formulations

The numerical method adopted in this study is grounded in the Reynolds-Averaged Navier–Stokes (RANS) equations, which are well established for modeling turbulent, incompressible flows around marine propellers. These equations provide the mathematical foundation for simulating the average

DOI: https://doi.org/10.11113/jurnalteknologi.v89.25357

effects of turbulence while maintaining reasonable computational demand.

Equation (5) denotes the momentum conservation equation, where the left-hand side includes both the convective transport of momentum and the contribution from turbulent fluctuations through Reynolds stresses, while the right-hand side incorporates the effects of pressure gradients and viscous or turbulent shear stresses that develop within the flow. Complementarily, Equation (6) represents the continuity equation, enforcing the conservation of mass by ensuring that the divergence of the velocity field remains zero throughout the domain—a constraint essential for maintaining physical accuracy in the numerical predictions [48,49].

$$\frac{\partial}{\partial x_j}\left(\rho\overline{u_i u_j} + \rho\overline{u_i'}\rho\overline{u_j'}\right) = -\frac{\partial \overline{p}}{\partial x_i} + \frac{\partial \overline{\tau_{ij}}}{\partial x_j} \quad (5)$$

$$\frac{\partial(\rho\overline{u_i})}{\partial x_i} = 0 \quad (6)$$

In this research, the RANS equations are solved using the Shear Stress Transport (SST) k-ω turbulence model, selected for its accuracy in handling adverse pressure gradients and flow separation—conditions commonly encountered in propeller flow simulations [50]. To account for surface roughness effects due to biofouling, the SST k-ω model is combined with a wall function approach [51]. This treatment allows for realistic representation of near-wall turbulence and shear stress without the need for excessive mesh refinement, thereby improving computational efficiency while maintaining predictive reliability [52].

2.3.2 Roughness Modeling

To account for the effects of surface roughness due to biofouling on the propeller surface, this study adopts a wall-function-based roughness model implemented in the turbulence closure framework. The model modifies the classical logarithmic law of the wall to include a roughness correction term, as shown in Equation (7). This formulation defines the dimensionless velocity profile U^+ in the near-wall region by incorporating a roughness function ΔU^+, which adjusts the velocity shift caused by the presence of rough surfaces [53].

$$U^+ = \frac{1}{\kappa}\ln(y^+) + B - \Delta U^+ \quad (7)$$

The roughness function ΔU^+, detailed in Equation (8), is governed by the dimensionless roughness height k_s^+ and transitions across three regimes: hydraulically smooth, transitionally rough, and fully rough. The function includes parameters such as A, C_s, and an exponent a, which is defined by a sine-based interpolation (Equation (9)) that ensures smooth blending between the transitional and rough regimes. This approach allows the model to flexibly capture the varying degrees of roughness encountered in biofouling scenarios without needing to resolve the physical texture of the fouled surface.

$$\Delta U^+ = \begin{cases} 0 & ; k_s^+ \le k_{s:S}^+ \\ \frac{1}{\kappa}\ln\left[A\left(\frac{k_s^+/k_{s:S}^+}{k_{s:R}^+ - k_{s:S}^+}\right) + C_s k_s^+\right]^a & ; k_{s:S}^+ < k_s^+ \le k_{s:R}^+ \\ \frac{1}{\kappa}\ln(\mathrm{A} + C_s k_s^+) & ; k_s^+ > k_{s:R}^+ \end{cases} \quad (8)$$

$$a = \sin\left[\frac{\pi}{2}\frac{\log(k_s^+/k_{s:S}^+)}{\log(k_{s:R}^+/k_{s:S}^+)}\right] \quad (9)$$

The parameters used in this study follow the calibration proposed by Cebeci and Bradshaw [54] and further adopted in modern CFD codes such as ANSYS Fluent: $A = 0$, $k_{s:S}^+$ (smooth) $= 2.25$, $k_{s:R}^+$ (rough) $= 90.00$, and $C_s = 0.253$. This rough wall function enables an accurate yet computationally efficient prediction of wall shear stress and near-wall velocity gradients, which are critical in evaluating the performance degradation of biofouled marine propellers.

2.3.3 Computational Domain and Boundary Conditions

To simulate the propeller flow field, a cylindrical computational domain was constructed with dimensions large enough to minimize blockage effects and ensure stable boundary interactions as described in Figure 3**Error! Reference source not found.**. The upstream (inlet) boundary was placed at a distance of 5 times the propeller diameter (5D), while the downstream (outlet) boundary extended to 13D behind the propeller. This setup ensures that both inflow development and wake dissipation occur sufficiently far from the propeller region, preventing artificial reflections and flow recirculation near the boundaries.

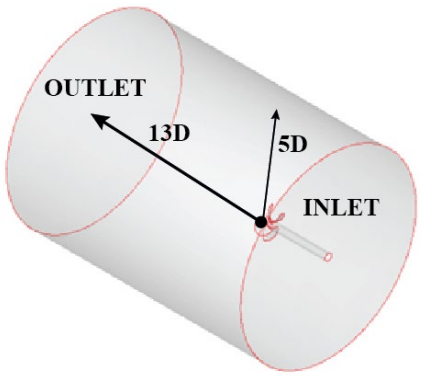


Figure 3 Computational domain and boundary condition configuration used in the simulation, showing the uniform velocity inlet at 5D upstream, pressure outlet at 13D downstream, and symmetry boundary condition applied on the lateral surface of the cylindrical domain

In the present study, a uniform velocity inlet was applied for all open-water performance simulations to

DOI: https://doi.org/10.11113/jurnalteknologi.v89.25357

prescribe the advance velocity corresponding to the selected advance coefficients, while the outlet was modeled as a pressure outlet with constant static pressure. The lateral surface of the cylindrical computational domain was defined as a symmetry boundary condition to avoid artificial wall effects and to represent an unbounded open-water environment. The propeller was modeled using a rotating reference frame, and steady-state simulations based on the Multiple Reference Frame (MRF) approach were employed for all parametric performance evaluations reported in this paper. Transient simulations using a sliding mesh approach and a total pressure inlet were conducted only for preliminary numerical checks and flow stability assessment and are not included in the performance results discussed in this study.

The chosen domain size and boundary settings follow best practices recommended by ITTC and previous propeller simulation studies (ITTC, 2011; Carlton, 2019), ensuring numerical stability and physical accuracy in capturing the flow characteristics around the propeller, especially in the presence of roughness-induced turbulence due to biofouling.

2.3.4 Grid Generation

A high-quality mesh is essential for accurately capturing the complex flow phenomena around the propeller, especially in regions affected by surface roughness and near-wall turbulence. In this study, a hybrid mesh topology was employed, combining structured hexahedral elements in the far-field domain and unstructured tetrahedral elements around the propeller blades and hub to accommodate geometric complexity.

Refinement was concentrated in the vicinity of the blade surfaces and the wake region to resolve boundary layer development, pressure gradients, and wake vortex structures. A prism layer was applied near the propeller surface to ensure adequate resolution of the wall-normal direction and to maintain appropriate y^+ values for wall function compatibility. This layer is particularly important in simulations involving roughness modeling, where accurate prediction of wall shear stress is critical.

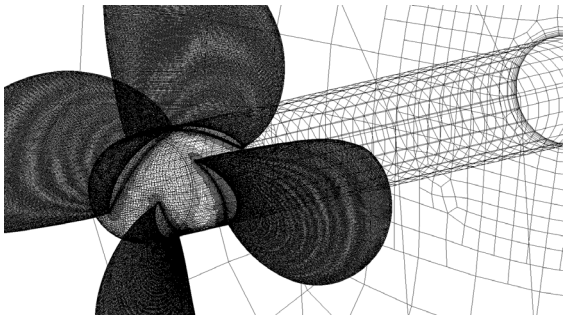


Figure 4 Surface and volume mesh structure around the propeller and downstream flow domain, consisting of approximately 2.3 million elements

The overall mesh consisted of approximately 2.3 million elements, as illustrated in Figure 4. Mesh independence was verified through a sensitivity analysis to ensure that the selected mesh resolution yields stable and accurate results without excessive computational cost. The mesh generation process followed best practices recommended in CFD guidelines for marine propeller simulations [50,55].

It should be noted that cavitation effects were not considered in the present simulations. The study focuses on non-cavitating open-water conditions in order to isolate the hydrodynamic impact of biofouling-induced surface roughness on propeller performance. The operating conditions investigated correspond to typical non-cavitating regimes of the Wageningen B-series propeller. While cavitation may further affect thrust and torque under certain operating conditions, its exclusion in this study does not alter the relative performance trends associated with surface roughness. Future work may extend the present approach to include cavitation modelling for a more comprehensive assessment.

3.0 RESULTS AND DISCUSSION

3.1 Verification

To ensure the numerical accuracy and reliability of the simulation results, a mesh independence (or grid convergence) study was conducted. This involved performing simulations using five different mesh densities, ranging from approximately 0.66 million to 5.18 million elements. The torque coefficient ($\boldsymbol{K_Q}$) was selected as the verification variable, and the percentage deviation between successive mesh results was calculated using the relative error formula shown in Equation (10).

$$\varepsilon = \frac{\left|R_{T_{(n+1)}} - R_{T_{(n)}}\right|}{R_{T_{(n)}}} \times 100\% \quad (10)$$

Table 3 Mesh convergence study based on torque coefficient ($\boldsymbol{K_Q}$) and relative error (ε) for different mesh densities

Mesh number	K_Q	ε
661.992	0.0784	-
1.028.208	0.0776	1.03%
2.332.956	0.0769	0.91%
3.643.380	0.0766	0.39%
5.182.134	0.0762	0.52%

As presented in Table 3, the variation in K_Q becomes progressively smaller with mesh refinement, indicating convergence. The relative error (ε) dropped below 1% after the second mesh level and reached a minimum

DOI: https://doi.org/10.11113/jurnalteknologi.v89.25357

of 0.39% at approximately 3.6 million elements. Beyond this point, further refinement had minimal effect on the results, suggesting that mesh convergence was achieved. Based on this analysis, the mesh with approximately 2.3 million elements was selected for all subsequent simulations, balancing computational efficiency and accuracy.

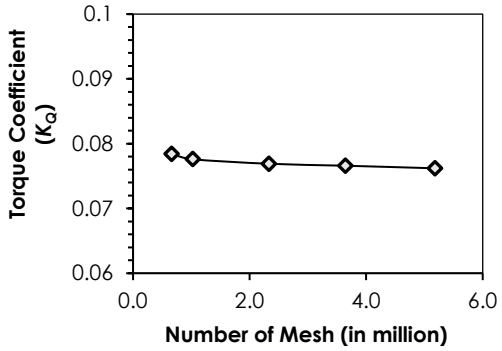


Figure 5 Variation of torque coefficient (K_Q) with increasing mesh number, showing mesh independence trend

Figure 5 illustrates the trend of the torque coefficient (K_Q) against the number of mesh elements, demonstrating a plateau behavior as the mesh becomes progressively finer. The initial decrease in K_Q values stabilizes beyond approximately 2 million elements, indicating that further refinement has a negligible effect on the results. This convergence behavior confirms that the selected mesh density is sufficient to capture the essential flow features with acceptable numerical accuracy, without incurring unnecessary computational cost.

3.2 Validation

To validate the accuracy of the numerical model, the CFD simulation results were compared with the experimental data from the Wageningen B-series propeller test [56]. The validation focuses on three performance parameters: thrust coefficient (K_T), torque coefficient (K_Q), and open water efficiency (η), evaluated across a range of advance coefficients (J).

As shown in Figure 6, the trends of the CFD predictions closely follow those of the experimental data for all three performance indicators. The thrust coefficient and torque coefficient exhibit consistent decline with increasing J, while the efficiency curve reaches a peak near the optimal operating point. Polynomial trend lines for the experimental data and CFD results illustrate strong agreement, especially in the mid-range of operation.

The quantitative comparison is presented in Table 4 and Table 5, showing the computed percentage error (E_ψ) using the formula in Equation (11). For thrust coefficient (K_T), the average error is 3.64%, while for torque coefficient (K_Q), the average error is 1.12%. Therefore, the average error is assumed to be 2.38%. These low error values indicate that the simulation is in good agreement with the reference data, confirming the validity of the numerical setup—including mesh resolution, turbulence modeling, and wall treatment—for predicting the propeller's open water performance.

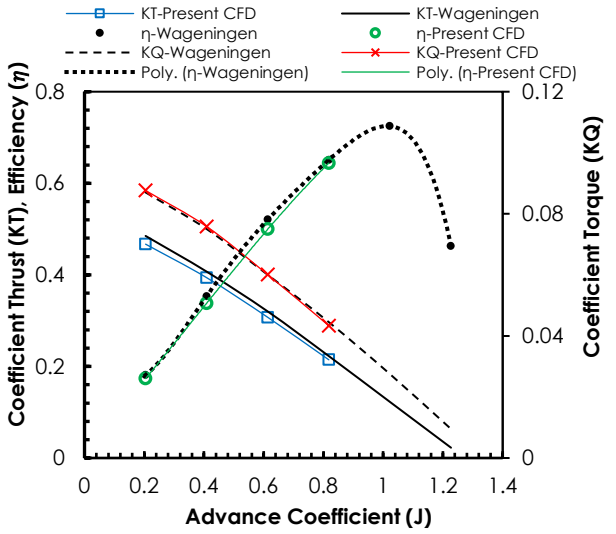


Figure 6 Comparison of thrust coefficient (K_T), torque coefficient (K_Q), and open water efficiency (η) between present CFD results and Wageningen B-series experimental data across various advance coefficients (J)

$$E_\psi\% = \left|\frac{\psi_{\text{CFD}} - \psi_{\text{experiment}}}{\psi_{\text{experiment}}}\right| \times 100\% \quad (11)$$

Table 4 Validation of thrust coefficient (K_T) between CFD simulation and Wageningen B-series data with corresponding percentage error (E_ψ%)

K_T-Wageningen [a]	K_T-Present CFD	E_ψ
0.485	0.467	3.70%
0.407	0.394	3.24%
0.320	0.307	3.99%
0.223	0.214	3.63%
Average		3.64%

[a] [56]

Table 5 Validation of torque coefficient (K_Q) between CFD simulation and Wageningen B-series data with corresponding percentage error (E_ψ%)

K_Q-Wageningen [a]	K_Q-Present CFD	E_ψ
0.087	0.088	0.71%
0.075	0.076	1.10%
0.060	0.060	0.07%
0.045	0.043	2.60%
Average		1.12%

[a] [56]

DOI: https://doi.org/10.11113/jurnalteknologi.v89.25357

3.3 Thrust changes due to roughness

The presence of surface roughness on the propeller blades, commonly caused by biofouling, has a significant impact on thrust generation. Figure 7 shows a comparison of the thrust coefficient (K_T) between a smooth surface and rough surfaces with different roughness heights (k_s=100, 300, and 500 µm) across a range of advance coefficients (J). In all cases, K_T decreases with increasing J, and the addition of surface roughness consistently results in a further decline in thrust performance.

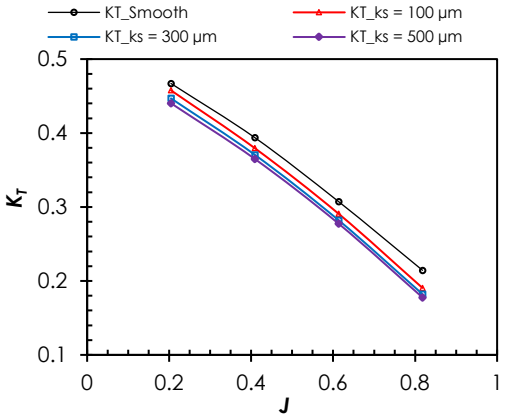


Figure 7 Comparison of thrust coefficient (K_T) for smooth and rough propeller surfaces at various roughness heights over a range of advance coefficients (J)

To evaluate this effect more clearly, Figure 8 presents the percentage reduction in thrust coefficient ($\Delta K_T\%$) relative to the smooth condition, calculated using Equation (12). The figure indicates a clear trend: the greater the roughness height, the larger the thrust loss. At a roughness height of 500 µm, the decrease in thrust reaches nearly 18% at higher J values, highlighting the severity of biofouling effects under light loading conditions.

$$\Delta K_T\% = \frac{\left(K_{T|(k_s)} - K_{T|(k_s=0)}\right)}{K_{T|(k_s=0)}} \times 100\% \qquad (12)$$

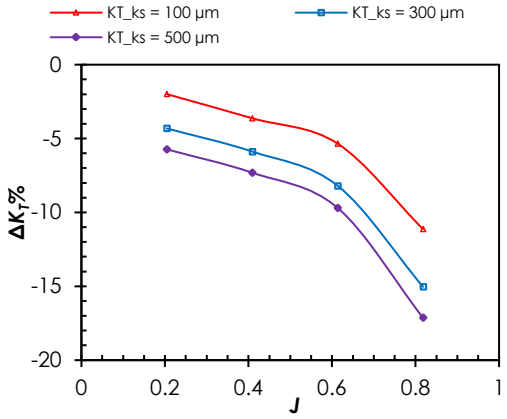


Figure 8 Percentage reduction in thrust coefficient ($\Delta K_T\%$) due to surface roughness relative to the smooth condition, indicating increasing thrust loss with higher roughness and increasing J

The underlying cause of this performance degradation is further illustrated in Figure 9 and Figure 10. Figure 9 shows the distribution of normal pressure on the suction and pressure sides of the propeller blades. For the rough surface (k_s=500µm), the pressure on the pressure side increases slightly, while the suction on the suction side is noticeably reduced. This imbalance leads to a lower pressure differential across the blade surfaces, directly resulting in diminished thrust.

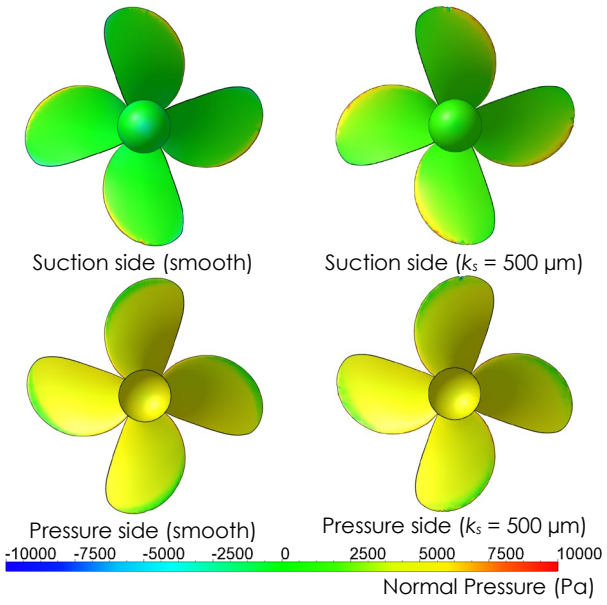


Figure 9 Normal pressure distribution on suction and pressure sides of the propeller blades, showing pressure increase and suction reduction due to surface roughness

Figure 10 highlights the wall shear stress distribution, showing increased shear on both the suction and pressure sides for the rough condition. The added roughness enhances turbulent momentum exchange

DOI: https://doi.org/10.11113/jurnalteknologi.v89.25357

near the wall, increasing frictional losses and promoting earlier boundary layer separation—particularly on the suction side where adverse pressure gradients are more sensitive.

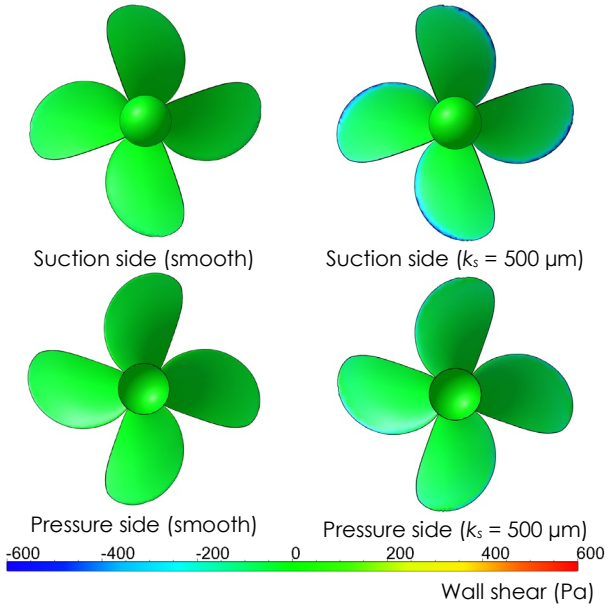


Figure 10 Wall shear stress distribution on both sides of the propeller, indicating higher shear levels in rough surface conditions

The reduction in thrust coefficient observed in the present study with increasing surface roughness is consistent with findings reported in recent numerical and experimental investigations on biofouled propellers. Previous studies have shown that biofouling alters the near-wall flow structure and boundary-layer development, leading to a reduced pressure difference between the suction and pressure sides of the blade and, consequently, a decrease in thrust generation [32,33,57]. Similar trends have been reported for Wageningen B-series and other conventional propellers, where thrust degradation becomes more pronounced at higher advance coefficients under light-loading conditions [32,33]. The present results reinforce these observations and indicate that, although surface roughness modifies the pressure distribution on the blade surface, its influence on thrust is relatively moderate compared to its impact on friction-related losses.

In summary, surface roughness caused by biofouling leads to increased wall shear stress and reduced pressure differential across the propeller blades, which together contribute to significant thrust loss. The severity of this effect scales with the roughness height and is most pronounced at higher advance coefficients, underscoring the importance of maintaining a smooth propeller surface for efficient operation.

3.4 Torque changes due to roughness

Surface roughness on propeller blades due to biofouling affects not only thrust generation but also the torque required to rotate the propeller. Figure 11 illustrates the variation of the torque coefficient (K_Q) with advance coefficient (J) for both smooth and rough surfaces (with k_s=100, 300, and 500 μm). It can be observed that K_Q generally decreases with increasing J, but the rough surfaces consistently produce higher K_Q values compared to the smooth condition.

This effect is quantified in Figure 12, which shows the percentage increase in torque coefficient (ΔK_Q%) due to surface roughness relative to the smooth condition. The results indicate a clear trend: as the roughness height increases, the torque also increases. At a roughness height of 500 μm, the torque rise exceeds 10% at high J values, highlighting the severity of biofouling under light loading conditions.

Figure 13 presents the distribution of normal pressure on the propeller blade surface. In this study, the term "normal pressure" refers to the static pressure component acting normal to the propeller blade surface, which directly contributes to the pressure difference between the suction and pressure sides and thus to thrust generation. This quantity is distinct from dynamic or total pressure, as it represents only the surface pressure loading resolved in the direction normal to the blade surface. The rough condition generates higher pressure levels than the smooth surface, contributing to increased resistance and hence higher torque requirements.

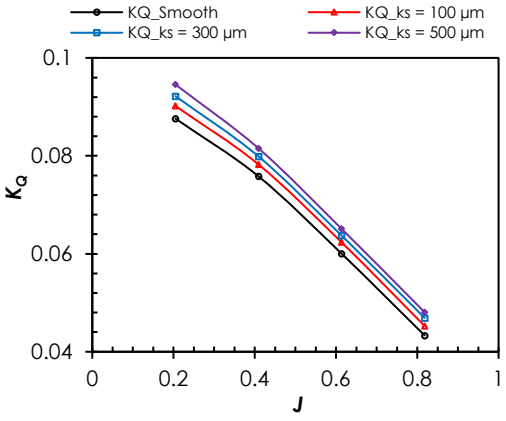


Figure 11 Comparison of torque coefficient (K_Q) for smooth and rough propeller surfaces at various roughness heights over a range of advance coefficients (J)

DOI: https://doi.org/10.11113/jurnalteknologi.v89.25357

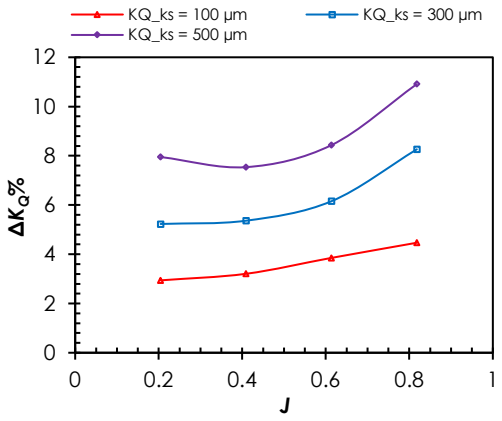


Figure 12 Percentage increase in torque coefficient ($\Delta K_Q\%$) due to surface roughness relative to the smooth condition

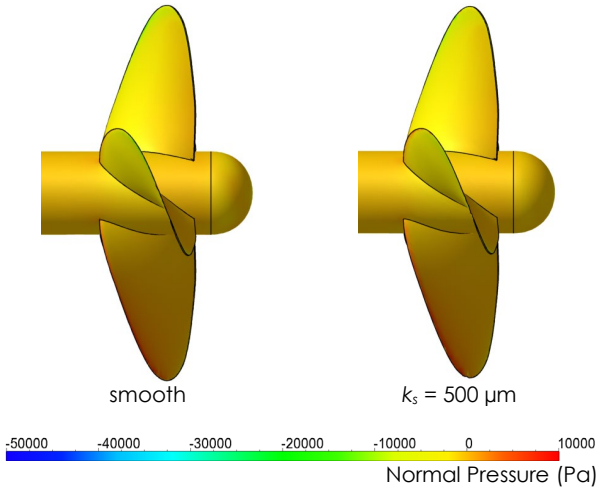


Figure 13 Normal pressure distribution on the propeller blade surface for smooth and rough conditions, showing elevated pressure levels in the rough surface

Moreover, Figure 14 shows the wall shear stress distribution, where the rough blade exhibits significantly higher shear stress compared to the smooth one. This increase aligns with the elevated frictional resistance, which adds to the overall torque demand.

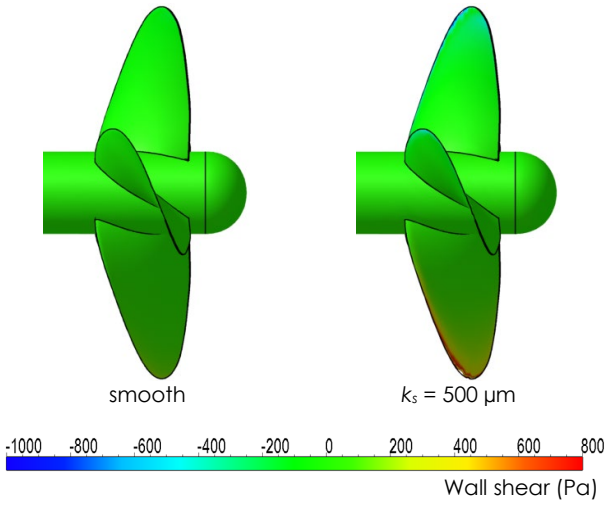


Figure 14 Wall shear stress distribution on the propeller surface, indicating significantly higher shear stress on the rough blade

The increase in torque coefficient with surface roughness obtained in this study agrees well with recent CFD-based investigations on propeller fouling. Several authors have reported that biofouling-induced roughness significantly enhances wall shear stress and turbulent momentum exchange near the blade surface, resulting in increased viscous resistance and higher torque demand [32,33,57]. The present results confirm that torque is more sensitive to surface roughness than thrust, particularly at higher advance coefficients, where frictional effects dominate the overall hydrodynamic response. This behavior is consistent with previous findings indicating that the primary penalty of propeller roughness manifests as an increase in required shaft power rather than a proportional reduction in thrust [32,33].

In summary, this subsection demonstrates that surface roughness caused by biofouling significantly increases the torque required by the propeller, which in turn may impact engine performance and fuel consumption.

3.5 Efficiency changes due to roughness

Surface roughness on propeller blades, typically caused by biofouling, has a direct influence not only on thrust and torque but also on overall propulsive efficiency. Figure 15 illustrates the variation of open water efficiency (η) for both smooth and rough surface conditions across various advance coefficients (J). As expected, η increases with J for all cases, indicating improved efficiency at higher advance ratios. However, the presence of surface roughness consistently lowers the efficiency compared to the smooth condition, with a more pronounced gap observed at higher values of J.

To further quantify this impact, Figure 16 presents the percentage reduction in efficiency ($\Delta\eta\%$) relative to

DOI: https://doi.org/10.11113/jurnalteknologi.v89.25357

the smooth condition. It is evident that greater surface roughness height leads to more significant efficiency losses. At a roughness height of 500 μm, the efficiency drop approaches nearly 25% at the highest tested J value. This trend reflects the compounded adverse effects of increased frictional resistance and disturbed flow over the blade surface due to roughness, which reduce the effective conversion of torque into useful thrust.

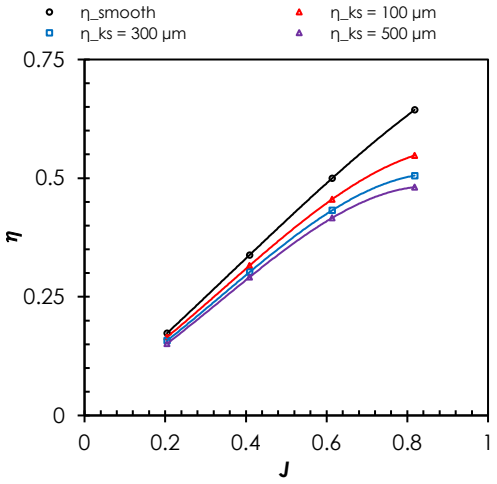


Figure 15 Comparison of open water efficiency (η) for smooth and rough propeller surfaces at different roughness heights over a range of advance coefficients (J)

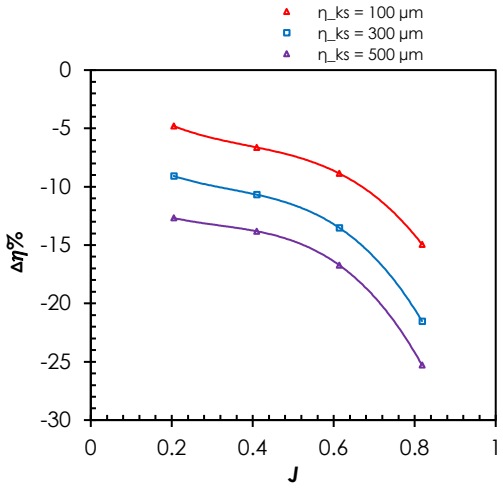


Figure 16 Percentage reduction in open water efficiency ($\Delta\eta$%) due to surface roughness, showing greater efficiency loss at higher advance coefficients and roughness levels

The combined effect of thrust reduction and torque increase leads to a notable decrease in open-water efficiency, as observed in the present study. This trend is in close agreement with recent experimental and numerical studies, which consistently report efficiency degradation as one of the most significant consequences of propeller biofouling [32,33,57]. Previous research has demonstrated that efficiency losses are largely governed by increased frictional resistance rather than changes in pressure-induced thrust, particularly under cruising or light-load operating conditions [32,33]. The present findings support this understanding, showing that surface roughness has a more pronounced impact on efficiency at higher advance coefficients, where even moderate roughness levels can result in substantial hydrodynamic performance penalties.

These findings underscore the critical role of maintaining clean and smooth propeller surfaces to minimize hydrodynamic losses and optimize propulsion efficiency, especially during light-loading conditions where J is high.

4.0 CONCLUSION

This study investigated the hydrodynamic impacts of biofouling-induced surface roughness on a widely used commercial marine propeller (B-series B4-70), focusing on changes in thrust, torque, and open water efficiency. By applying a wall-function-based roughness model within a validated RANS-SST CFD framework, the research successfully captured the complex interactions between blade surface conditions and flow behavior without requiring fully resolved roughness geometries.

The results indicate that surface roughness significantly degrades propeller performance. Thrust coefficient (K_T) consistently decreased as roughness height increased, with the worst-case condition (k_s= 500 μm) showing up to 18% thrust loss at high advance coefficients. Simultaneously, torque coefficient (K_Q) increased due to elevated wall shear stress and pressure buildup on the blade surfaces, resulting in more than 10% torque penalty under the same conditions.

These thrust and torque changes cumulatively reduced open water efficiency (η), particularly at higher advance coefficients where flow separation and boundary layer disturbance were more pronounced. The efficiency drop reached nearly 25%, underscoring how even moderate biofouling can lead to substantial energy losses.

In conclusion, biofouling on the propeller not only increases fuel consumption and emissions but also reduces operational efficiency, especially during cruising or light-load conditions. Maintaining clean and smooth propeller surfaces is essential for optimizing ship propulsion performance, minimizing fuel usage, and supporting broader emission reduction targets in maritime operations.

Acknowledgement

This research was funded by Riset Publikasi Internasional (RPI) as research funding scheme from Institute for Research and Community Services (LPPM), Diponegoro University 2025 research scheme with contract number 222-589/UN7.D2/PP/IV/2025.

Conflicts of Interest

The authors declare that there is no conflict of interest regarding the publication of this paper.

Data availability

The data supporting the findings of this study are available from the corresponding author upon reasonable request.

Ethics declaration

Formal ethical approval was not obtained for this study. However, the authors confirm that the research was conducted in accordance with established ethical principles and good research practices, with due consideration given to participant rights, informed consent, confidentiality, and responsible data handling.

References

[1] Hakim ML, Tuswan, Firdaus A, Mursid O. Investigating the Comparison of Ship Resistance Components Between U and V-Shaped Hulls. Jurnal Teknologi 2023;85:153–64. https://doi.org/10.11113/jurnalteknologi.v85.19382.

[2] Choi HJ. Hull-form optimization of a container ship based on bell-shaped modification function. International Journal of Naval Architecture and Ocean Engineering 2015;7:478–89. https://doi.org/10.1515/ijnaoe-2015-0034.

[3] Haase M. Energy-efficient large medium-speed catamarans: Hull form design by full-scale CFD simulations. Ship Technology Research 2016;63:133–4. https://doi.org/10.1080/09377255.2016.1208974.

[4] Trimulyono A, Hakim ML, Ardhan C, Ahmad STP, Tuswan T, Santosa AWB. Analysis of the double steps position effect on planing hull performances. Brodogradnja 2023;74:41–72. https://doi.org/10.21278/brod74403.

[5] Radonja R, Pavić D, Glujić D. Methodological approach on optimizing the speed of navigation to reduce fuel consumption and increase energy efficiency of the cruising ship. Pomorstvo 2019;33:222–31. https://doi.org/10.31217/p.33.2.12.

[6] Farkas A, Degiuli N, Martić I, Vujanović M. Greenhouse gas emissions reduction potential by using antifouling coatings in a maritime transport industry. Journal of Cleaner Production 2021;295. https://doi.org/10.1016/j.jclepro.2021.126428.

[7] Adietya BA, Syahab H, Indiaryanto M, Aryawan WD, Utama IKAP. Influence Evaluation of Open Propellers with Boss Cap Fins: Case Studies on Types B4-70 and Ka4-70. CFD Letters 2024;16:143–77. https://doi.org/10.37934/cfdl.16.9.143177.

[8] Arifin MD, Felayati FM, Muhammad AH. Flow Separation Evaluation on Tubercle Ship Propeller. CFD Letters 2022;14:43–50. https://doi.org/10.37934/cfdl.14.4.4350.

[9] Berlian Arswendo Adietya, I Ketut Aria Pria Utama, Wasis Dwi Aryawan, Dwi Wahyudi, Anis Kurniati Arifah, Baharuddin Ali, et al. Characteristics Investigations of Ducted Ka4-70 Series Propeller with Boss Cap Fins Using Numerical and Experimental Method. CFD Letters 2023;16:24–41. https://doi.org/10.37934/cfdl.16.2.2441.

[10] Corbett JJ, Fischbeck PS, Pandis SN. Global nitrogen and sulfur inventories for oceangoing ships. Journal of Geophysical Research: Atmospheres 1999;104:3457–70. https://doi.org/10.1029/1998JD100040.

[11] Felayati FM, Semin, Cahyono B, Bakar RA, Birouk M. Performance and emissions of natural gas/diesel dual-fuel engine at low load conditions: Effect of natural gas split injection strategy. Fuel 2021;300:121012. https://doi.org/10.1016/j.fuel.2021.121012.

[12] Taskar B, Andersen P. Benefit of speed reduction for ships in different weather conditions. Transportation Research Part D: Transport and Environment 2020;85:102337. https://doi.org/10.1016/j.trd.2020.102337.

[13] Bigi N, Roncin K, Leroux J-B, Parlier Y. Ship Towed by Kite: Investigation of the Dynamic Coupling. Journal of Marine Science and Engineering 2020;8:486. https://doi.org/10.3390/jmse8070486.

[14] Podeur V, Merdrignac D, Behrel M, Roncin K, Fonti C, Jochum C, et al. Fuel economy assessment tool for auxiliary kite propulsion of merchant ship. La Houille Blanche 2018;104:5–7. https://doi.org/10.1051/lhb/2018001.

[15] Josten F, Isensee J. Design aspects of solar-powered ships. Ship Technology Research 1998.

[16] Nasirudin A, Hasanudin H, Utama D, Tahwoto LP. Determination of PV Power and Battery Capacity Size for a Leisure Solar Powered Boat at Kalimas River, Surabaya, Indonesia. Kapal: Jurnal Ilmu Pengetahuan Dan Teknologi Kelautan 2020;17:123–9. https://doi.org/10.14710/kapal.v17i3.31965.

[17] Schultz MP, Bendick JA, Holm ER, Hertel WM. Economic impact of biofouling on a naval surface ship. Biofouling 2011;27:87–98. https://doi.org/10.1080/08927014.2010.542809.

[18] Hakim ML, Nugroho B, Nurrohman MN, Suastika IK, Utama IKAP. Investigation of fuel consumption on an operating ship due to biofouling growth and quality of anti-fouling coating. IOP Conference Series: Earth and Environmental Science 2019;339:012037. https://doi.org/10.1088/1755-1315/339/1/012037.

[19] Hakim ML, Suastika IK, Utama IKAP, Purnamasari D, Muryadin M. Frictional Resistance Increase Due to Hull Roughness: An Analysis of the Hull Form Parameters Influence. Transactions on Maritime Science 2023;12. https://doi.org/10.7225/toms.v12.n02.002.

[20] Oliveira D, Granhag L. Matching Forces Applied in Underwater Hull Cleaning with Adhesion Strength of Marine Organisms. Journal of Marine Science and Engineering 2016;4:66. https://doi.org/10.3390/jmse4040066.

[21] Oliveira DR, Lagerström M, Granhag L, Werner S, Larsson AI, Ytreberg E. A novel tool for cost and emission reduction related to ship underwater hull maintenance. Journal of Cleaner Production 2022;356:131882. https://doi.org/10.1016/j.jclepro.2022.131882.

[22] Schultz MP. Effects of coating roughness and biofouling on ship resistance and powering. Biofouling 2007;23:331–41. https://doi.org/10.1080/08927010701461974.

[23] Demirel YK, Turan O, Incecik A. Predicting the effect of biofouling on ship resistance using CFD. Applied Ocean Research 2017;62:100–18. https://doi.org/10.1016/j.apor.2016.12.003.

[24] Hakim ML, Firdhaus A, Samuel S, Song S, Kim S, Utama IKAP.

Investigating the impact of inhomogeneous roughness on the drag of a planing craft assisted by numerical simulation. Ocean Engineering 2025;325:120826. https://doi.org/10.1016/j.oceaneng.2025.120826.
[25] Amiruddin W, Hakim ML, Firdhaus A, Purnamasari D, Tuswan T, Samuel S, et al. Prediction of the impact of biofouling roughness on a full-scale planing boat performance using CFD. Ocean Engineering 2024;301:117457. https://doi.org/10.1016/j.oceaneng.2024.117457.
[26] Amiruddin W, Hakim ML, Fernanda R, Firdhaus A, Purnamasari D, Samuel S, et al. Assessing drag increase on fishing vessels due to biofouling-induced surface roughness using CFD. Ships and Offshore Structures 2025:1–17. https://doi.org/10.1080/17445302.2025.2472266.
[27] Schultz MP, Kavanagh CJ, Swain GW. Hydrodynamic forces on barnacles: Implications on detachment from fouling-release surfaces. Biofouling 1999;13:323–35. https://doi.org/10.1080/08927019909378388.
[28] Vijayanandh R, Venkatesan K, Raj Kumar R, Senthil Kumar M, Raj Kumar G, Jagadeeshwaran P. Theoretical and Numerical Analyses on Propulsive Efficiency of Unmanned Aquatic Vehicle's Propeller. Journal of Physics: Conference Series 2020;1504:012004. https://doi.org/10.1088/1742-6596/1504/1/012004.
[29] Fish FE. Advantages of Natural Propulsive Systems. Marine Technology Society Journal 2013;47:37–44. https://doi.org/10.4031/MTSJ.47.5.2.
[30] Song S, Demirel YK, Atlar M. An investigation into the effect of biofouling on full-scale propeller performance using CFD. Proceedings of the International Conference on Offshore Mechanics and Arctic Engineering - OMAE, vol. 2, American Society of Mechanical Engineers; 2019. https://doi.org/10.1115/OMAE2019-95315.
[31] Song S, Demirel YK, Atlar M. Penalty of hull and propeller fouling on ship self-propulsion performance. Applied Ocean Research 2020;94:102006. https://doi.org/10.1016/j.apor.2019.102006.
[32] Farkas A, Degiuli N, Martić I. The impact of biofouling on the propeller performance. Ocean Engineering 2021;219:108376. https://doi.org/10.1016/j.oceaneng.2020.108376.
[33] Owen D, Demirel YK, Oguz E, Tezdogan T, Incecik A. Investigating the effect of biofouling on propeller characteristics using CFD. Ocean Engineering 2018;159:505–16. https://doi.org/10.1016/j.oceaneng.2018.01.087.
[34] Seo K-C, Atlar M, Goo B. A Study on the Hydrodynamic Effect of Biofouling on Marine Propeller. Journal of the Korean Society of Marine Environment and Safety 2016;22:123–8. https://doi.org/10.7837/kosomes.2016.22.1.123.
[35] Zinati A, Ketabdari MJ, Zeraatgar H. Effects of Propeller Fouling on the Hydrodynamic Performance of a Marine Propeller. Polish Maritime Research 2023;30:61–73. https://doi.org/10.2478/pomr-2023-0059.
[36] Marcus EA, de Vries R, Raju Kulkarni A, Veldhuis LL. Aerodynamic Investigation of an Over-the-Wing Propeller for Distributed Propulsion. 2018 AIAA Aerospace Sciences Meeting, Reston, Virginia: American Institute of Aeronautics and Astronautics; 2018. https://doi.org/10.2514/6.2018-2053.
[37] Liu Y, Li L, Ning Z, Tian W, Hu H. Experimental Investigation on the Dynamic Icing Process over a Rotating Propeller Model. Journal of Propulsion and Power 2018;34:933–46. https://doi.org/10.2514/1.B36748.
[38] Zhang J, Wang J, Zhang B, Zeng Y, Duan J, Hou B. Fabrication of anodized superhydrophobic 5083 aluminum alloy surface for marine anti-corrosion and anti-biofouling. Journal of Oceanology and Limnology 2020;38:1246–55. https://doi.org/10.1007/s00343-020-0036-3.
[39] Salta M, Wharton JA, Stoodley P, Dennington SP, Goodes LR, Werwinski S, et al. Designing biomimetic antifouling surfaces. Philosophical Transactions of the Royal Society A: Mathematical, Physical and Engineering Sciences 2010;368:4729–54. https://doi.org/10.1098/rsta.2010.0195.
[40] Chrismianto D, Zakki AF, Arswendo B, Cendikia Abar IA. Comparison of Propeller Type B-Series And AU-Outline Gawn Series For Improving On Submarine Propulsion Performance Using Cfd. International Journal Of Advanced Research In Engineering & Technology 2019;10. https://doi.org/10.34218/IJARET.10.2.2019.061.
[41] Kelly J, Vogel C, Willden R. Impact and mitigation of blade surface roughness effects on wind turbine performance. Wind Energy 2022;25:660–77. https://doi.org/10.1002/we.2691.
[42] Vecchia P Della, Malgieri D, Nicolosi F, De Marco A. Numerical analysis of propeller effects on wing aerodynamic: tip mounted and distributed propulsion. Transportation Research Procedia 2018;29:106–15. https://doi.org/10.1016/j.trpro.2018.02.010.
[43] Adietya BA, Aryawan WD, Utama IKAP. A study into the effect of tip clearance on the performance of b-series and kaplan-series ducted propellers. IOP Conference Series: Earth and Environmental Science 2023;1166:012038. https://doi.org/10.1088/1755-1315/1166/1/012038.
[44] Berlian Arswendo Adietya, I Ketut Aria Pria Utama, Wasis Dwi Aryawan, Mochammad Nasir, Nurcholis, Mahendra Indiaryanto, et al. Numerical and Experimental Investigations into the Characteristics of Wageningen B4-70 Series of Propeller with Boss Cap Fins. CFD Letters 2023;15:152–69. https://doi.org/10.37934/cfdl.15.10.152169.
[45] Berlian Arswendo Adietya, Husein Syahab, Mochammad Nasir, Wasis Dwi Aryawan, I Ketut Aria Pria Utama. Numerical Analysis into the Improvement Performance of Ducted Propeller by using Fins: Case Studies on Types B4-70 and Ka4-70. CFD Letters 2024;16:12–42. https://doi.org/10.37934/cfdl.16.10.1242.
[46] Carlton J. Marine Propellers and Propulsion. Elsevier; 2012. https://doi.org/10.1016/C2010-0-68327-1.
[47] Molland AF, Turnock SR, Hudson DA. Ship Resistance and Propulsion. Cambridge: Cambridge University Press; 2017. https://doi.org/10.1017/9781316494196.
[48] Versteeg HK, Malalasekera W. An Introduction to Computational Fluid Dynamics. 2nd ed. Edinburgh: Pearson Education; 2007.
[49] Wilcox DC. Turbulence modeling for CFD 1994:15–9.
[50] Menter FR. Two-equation eddy-viscosity turbulence models for engineering applications. AIAA Journal 1994;32:1598–605. https://doi.org/10.2514/3.12149.
[51] Flack KA, Schultz MP. Review of hydraulic roughness scales in the fully rough regime. Journal of Fluids Engineering, Transactions of the ASME 2010;132:0412031–04120310. https://doi.org/10.1115/1.4001492.
[52] ANSYS. Introduction to ANSYS Fluent. Lecture 7: Turbulence Modeling. ANSYS User Manual 2014.
[53] Hama F. Boundary-layer characteristics for smooth and rough surfaces. Transactions - The Society of Naval Architects and Marine Engineers 1954;62:333–58.
[54] Cebeci T, Bradshaw P. Momentum transfer in boundary layers. New York: Hemisphere Publishing Corporation; 1977.
[55] ITTC. 9.1.0__Practical Guidelines for Ship CFD Applications. ITTC – Recommended Procedures and Guidelines ITTC 2011:1–8.
[56] Bernitsas M., Ray D, Kinley P. KT, KQ and Efficiency curvers for Wag b-series. University of Michigan 1981.
[57] Song S, Demirel YK, Atlar M. Propeller performance penalty of biofouling: Computational fluid dynamics prediction. Journal of Offshore Mechanics and Arctic Engineering 2020;142. https://doi.org/10.1115/1.4047201.